

Uplift and a possible Moho offset across the Dead Sea transform

U.S. ten Brink^{a,b}, N. Schoenberg^b, R.L. Kovach^a and Z. Ben-Avraham^b

^a *Department of Geophysics, Stanford University, Stanford, CA 94305 (U.S.A.)*

^b *Department of Geophysics and Planetary Sciences, Tel Aviv University, Tel Aviv 69978 (Israel)*

(Revised version accepted June 1, 1989)

ABSTRACT

Ten Brink, U.S., Schoenberg, N., Kovach, R.L. and Ben-Avraham, Z., 1990. Uplift and a possible Moho offset across the Dead Sea transform. In: R.L. Kovach and Z. Ben-Avraham (Editors), *Geologic and Tectonic Processes of the Dead Sea Rift Zone*. *Tectonophysics*, 180: 71–85.

The East Africa rifts and the Red Sea spreading center are characterized by uplifted shoulders and sunken median valleys. The Dead Sea transform, on the northern extension of the Arabian–African plate boundary, has a similar morphological character despite its well-documented strike-slip motion. To understand the “rift” morphology and the crustal structure beneath the transform we compiled a 320 km long gravity and topography profile perpendicular to the Dead Sea transform. The gravity field and the topography in the region surrounding the profile are generally parallel to the trend of the Dead Sea transform, justifying the two-dimensional approximation of the analysis. The gravity profile was modeled using constraints from seismic refraction, borehole and surface geology data. The observed gravity anomaly can be explained by the juxtaposition of two different sedimentary and crustal sections which have been offset by a 105 km left-lateral displacement across the transform boundary, suggesting a step in the depth to Moho. The existence of a significant density anomaly under the median valley is not required by the model. The current elevation of the transform shoulders appears not to be compensated locally. Assuming a state of local isostasy prior to the development of the transform, the magnitude of the uplift in the vicinity of the profile is estimated at 700–900 m, with a half width of 100–125 km. This topography (uplift) can be fitted equally well by models which assume either dynamic support or regional compensation. It is suggested that if the source of the uplift is thermal, it is located within the upper mantle, since there is no requirement for a shallow density anomaly under the rift itself or in the crust nearby.

Introduction

Flank uplifts of ≥ 1 km are observed along many continental rifts and reveal insight into the rifting process. For example, the geographical and temporal associations of flank uplift with lithospheric extension are indicative of the thermal regime in the upper mantle under rifts and are used to differentiate between active and passive rifting processes (Steckler, 1985; Buck, 1986, Moretti and Chenet, 1987; Bohannon et al., 1989).

The southern half of the approximately 930 km long Dead Sea transform morphologically resembles a continental rift zone and has therefore been traditionally referred to as the Dead Sea Rift

(Bender, 1968; Dubertret, 1970). It is occupied by a 5–20 km wide median valley which is bounded in places by normal faults. Much of the length of the median valley, about 270 km, lies below sea level (Fig. 1). The southernmost 180 km of the transform, the Gulf of Aqaba (Elat), is composed of a series of submarine basins with a maximum water depth of 1600 m (Ben-Avraham et al., 1979). Both the median valley and the Gulf of Aqaba are surrounded by uplifted shoulders. The shape of the eastern shoulder is similar to the eastern shoulder of the Red Sea. It rises gently westward reaching its highest elevations near the transform and then drops abruptly into the median valley. The shape of the western shoulder varies along its

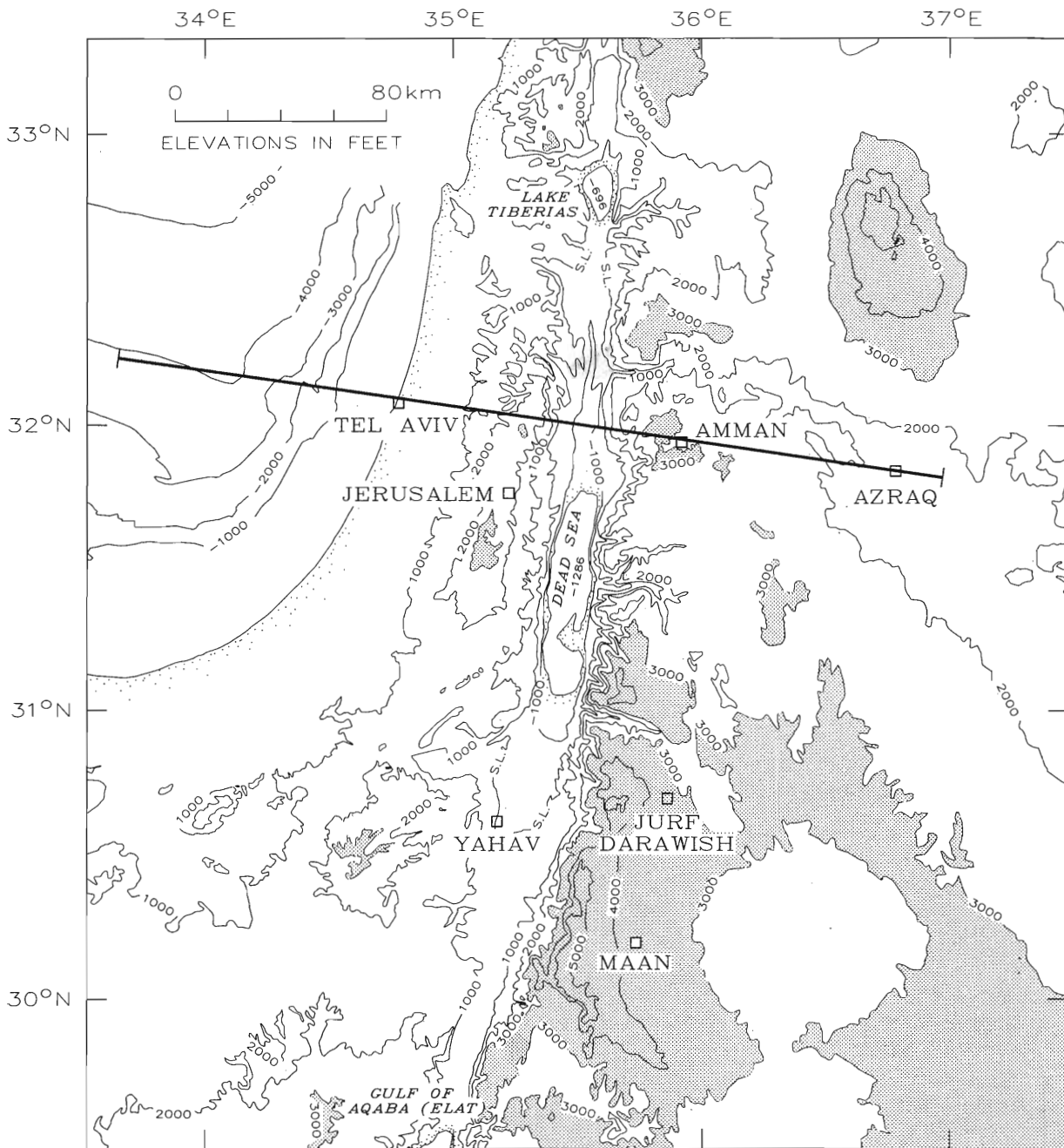


Fig. 1. Simplified topographic map of the Dead Sea transform and its surrounding region. Elevations were taken from MOD (1982) and DMA (1982) with a contour interval of 1000 ft. The location of a 320 km long gravity and topography profile is shown.

length and the highest elevations are not always close to the median valley. The elevation of the eastern shoulder is usually higher than that of the western shoulder, reaching 1500–2200 m south of 30°N and 800–1300 m further north. With the exception of the southern Sinai peninsula, the

western shoulder has a lower average elevation of 500–1200 m.

Despite the apparent morphological similarities with extensional rift zones such as the Gulf of Suez and the Red Sea, the Dead Sea transform has been convincingly shown to be dominated by left-

lateral strike-slip motion (Quennell, 1959; Freund et al., 1970), and perpendicular extensional motion is either minor or non-existent (Garfunkel, 1981). The evidence has come largely from comparing crystalline, volcanic, and sedimentary formations, ranging in age from Precambrian to Eocene, across the transform (Quennell, 1959; Freund, 1970). Further confirmation of sinistral movement has come from matching magnetic field patterns across the transform (Hatcher et al., 1981).

As some of the East African rifts have a significant component of horizontal displacement along them (Scott et al., 1989), the Dead Sea transform could be viewed as one end member of continental rifts, with major horizontal displacement and a negligible amount of extensions. There are, however, two additional observations which distinguish the Dead Sea transform from other continental rift systems: (1) the width of the median valley is only 5–20 km as compared to 40–60 km in other continental rifts such as the East African rift system, the Gulf of Suez, the Baikal, and the Rhine Graben and (2) the surface heat flow along the Dead Sea transform and its surrounding area does not deviate from the average global heat flow for the interior of the continents (Ben-Avraham et al., 1978; Feinstein, 1987; Galanis et al., 1986).

The question of whether and how continental transforms extend into the lower crust and upper mantle is not well documented. Partial or complete decoupling between the upper brittle layer and the lower ductile layer have been suggested below the seismogenic zone in the San Andreas fault zone (Lachenbruch and Sass, 1980; Furlong et al., 1989). Observations bearing on this question are complicated in most major continental transforms by their associated deformation due to collision or subduction (e.g., the San Andreas fault has been overprinted by the northward migration of the Mendocino Triple Junction). In contrast, the Dead Sea transform has been the site of a Jurassic passive continental margin (Bein and Gvirtzman, 1977). Thus, the chances of observing the extension of the transform to the lower crust and upper mantle along the Dead Sea are better than in other continental transforms.

The purpose of this paper is to investigate the

unique topographic expression of the Dead Sea transform and the structure of the underlying crust by analyzing a gravity and topography profile perpendicular to the transform. The degree of coherency between the topography, the gravity, and the derived Moho depth is used to discuss the lower crustal structure of the transform and possible uplift mechanisms for the rift shoulders. We are aware that it is preferable to perform this type of analysis using a set of profiles or a two-dimensional data set rather than analyzing a single profile. Unfortunately, the lack of gravity coverage across the median valley and political obstacles preclude such analysis at the present time. The gravity and topographic features to about 30 km (about one crustal thickness) on either side of the profile are, however, generally spatially uniform, giving credibility to the results of the analysis presented in this paper.

Gravity and topography profile

A 320 km long profile of the free-air gravity anomaly and topography across the Dead Sea transform is shown in Fig. 2. The profile passes through Azraq, Amman and Tel Aviv and is sub-parallel to latitude 32°N. The profile location was selected to avoid the deep pull-apart basins along the rift where there might be a question as to whether the gravity anomaly is caused by a thick sedimentary fill or by an underlying intrusion. The sedimentary thickness of the rift-filled sediments in the median valley in the vicinity of the profile is no more than 300 m (based on the Jordan Valley 1 borehole and seismic reflection sections; see Kashai and Crocker, 1987). The topographic profile was digitized from maps with a contour interval of 20 m. The gravity profile was compiled from the Bouguer gravity maps of Abu-Ajamieh (1973) and Folkman (1976) on land, from maps of commercial surveys in the Eastern Mediterranean Sea, and from data held at the archives of the Institute of Petroleum Research and Geophysics in Israel. The contour interval on most of the maps is 1 mGal but some areas with sparse data coverage have contours of 5 mGal. Because each of the maps was reduced with a different Bouguer density, the digitized data have been converted to

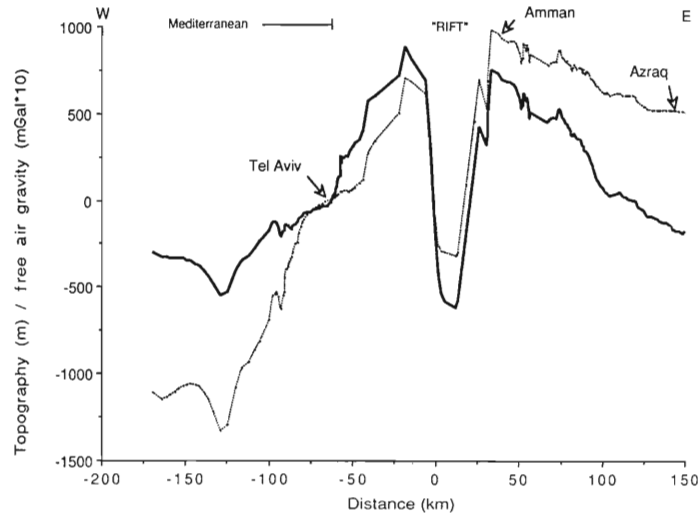


Fig. 2. Free-air gravity anomaly (heavy line) and topography (dotted line) along the profile located in Fig. 1.

free-air gravity anomalies. The conversion was performed by adding the effect of a slab with the assumed density assigned by the various studies, and thickness equal to the elevation of that point from the topographic map. Care was taken to match the different surveys and compare them with values of regional gravity stations, because the different surveys were reduced with different base values and gravity formulae. The uncertainty

of the match across the Dead Sea transform is estimated to be no worse than 5 mGal.

As expected, the free-air gravity and the topography profiles of Fig. 2 are well correlated. The general trend of westward decrease in elevation is not matched, however, by a comparable decrease in the free-air gravity anomaly. The elevation of the eastern shoulder of the rift is higher than the western shoulder while the associated gravity

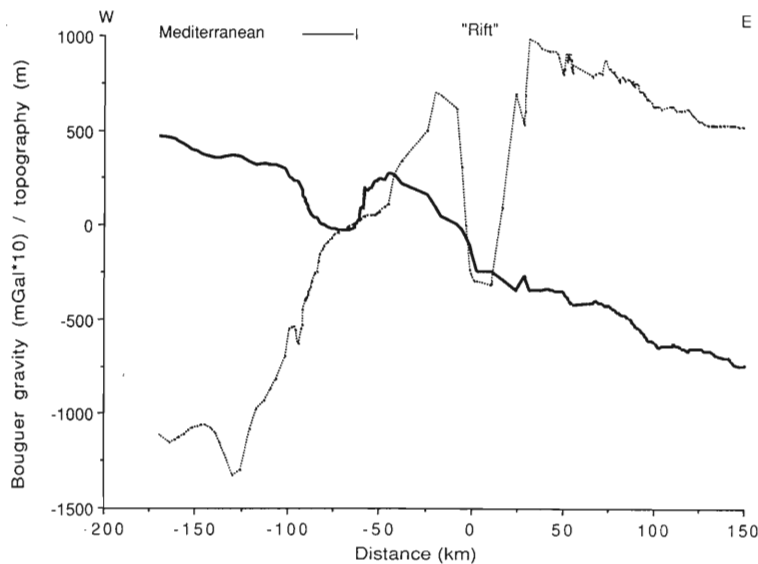


Fig. 3. Bouguer gravity anomaly (heavy line) and topography along the profile located in Fig. 1. The Bouguer gravity profile was obtained by applying a uniform reduction density of 2.67 g/cm^3 to the profile in Fig. 2.

anomaly is lower on the eastern shoulder than on the western shoulder.

A Bouguer correction with a uniform reduction density of 2.67 g/cm^3 was applied to the free-air profile to remove the contribution of the topography. The Bouguer correction reveals a long-wavelength trend of increasing Bouguer gravity anomaly from land toward the sea (Fig. 3). This increase is typical of continental margins around the world and is due to gradual thinning of the crust from continent to ocean. The main conclusion from the Bouguer gravity profile is that the Dead Sea transform in this vicinity is not associated with any sizable local anomaly. The lack of a gravity anomaly over the Dead Sea transform has been pointed out by previous studies (Folkman, 1980; Kovach and Ben-Avraham, 1985) which involved analysis of much shorter gravity profiles.

Gravity models

Figure 4 compares calculated results for the model presented in Fig. 5 and a gravity profile in which Bouguer anomalies are used above sea level and free-air anomalies below sea level. The contribution of the attracting mass above sea level was removed along the profile by applying Bouguer correction with variable densities: 2.55 g/cm^3 for

the Mesozoic carbonate platform which covers most of the profile above sea level, and 2.15 g/cm^3 for the Tertiary sediments on the coastal plain of Israel (Folkman, 1976). The fit between the calculated effect of the model and the gravity anomaly profile is good and the standard deviation of the differences between them is only 4.7 mGal. Differences are mostly for anomaly widths $\leq 50 \text{ km}$, and are probably due to unmodeled shallow variations in the local density structure.

The gravity data by themselves cannot be inverted to give a unique underlying density structure. The model in Fig. 5 was constructed using published estimates of the depths to different density interfaces from seismic refraction, magnetic, deep drilling and surface geology data (see references in the figure caption). Where estimates were not available, we used inference or assumed the simplest structure possible. For example, the gradual increase in crustal thickness from the Mediterranean basin eastward shown in Fig. 5 is based on seismic refraction results from further south (Ginzburg and Folkman, 1980). A second example is the assumption of a constant thickness for the low-density sediments in the continental slope and rise of the Mediterranean basin.

An interesting feature of the model is the lack of any detectable density anomaly associated with

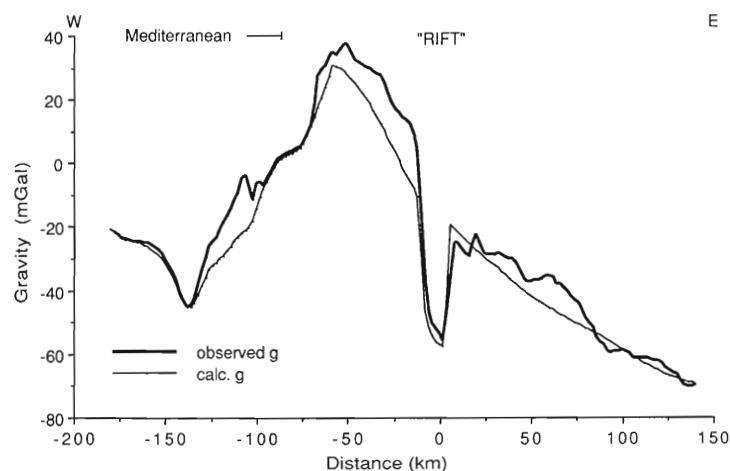


Fig. 4. Comparison between the calculated gravity anomaly from the model in Fig. 5 (thin line) and the gravity anomaly (heavy line). The gravity anomaly is composed of free-air anomaly below sea level (in the Mediterranean Sea and the median valley of the transform), and a Bouguer anomaly above sea level. The Bouguer gravity anomaly was reduced with near-surface measured rock densities (Folkman, 1976): 2.55 g/cm^3 for the Mesozoic carbonate platform which is exposed along most of the profile and 2.15 g/cm^3 along the coastal plain of Israel.

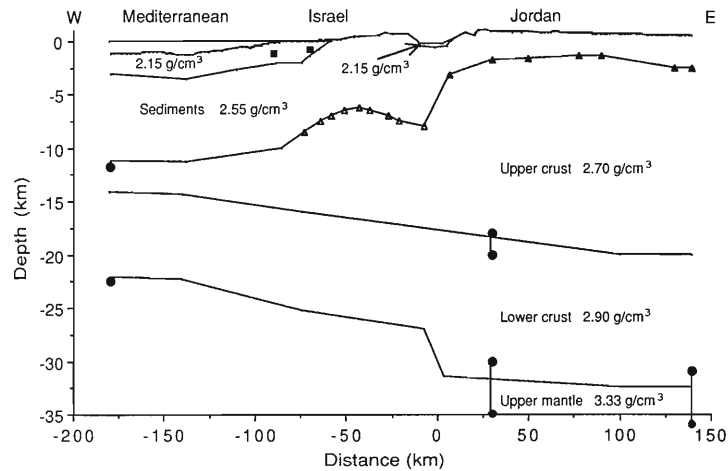


Fig. 5. The density model which was used to calculate the gravity anomaly in Fig. 4. The model was constructed using geological estimates of the depths to the various interfaces along the profile from the following sources: isopach maps (triangles, from Bender, 1968) and seismic refraction results (dots, El-Isa et al., 1987) under Jordan; seismic refraction results (triangles, Ginzburg and Folkman, 1981), deep boreholes (squares, O. Wolf, pers. commun., 1987) and a basement magnetic model (O. Wolf, pers. commun., 1987) under Israel; and seismic refraction results at sea (dots, Makris et al., 1983). Where estimates were not available, the model followed the simplest structure possible or the shape of interfaces from published estimates in adjacent areas (e.g., Ginzburg and Folkman, 1980).

the transform. In the model, two different crustal sections are simply juxtaposed against each other. The crust east of the rift is about 30 km thick and is fairly constant in thickness. The crust adjacent to the rift to the west is only 20 km thick and thins rapidly to about 11 km under the Mediterranean basin. These crustal variations are also qualita-

tively suggested by a change in the slope of the Bouguer gravity profile at the transform (Fig. 3).

The lack of a detectable density anomaly under the median valley of the transform corroborates previous seismic refraction results which were collected along the axis of the median valley south of the Dead Sea. The refraction results showed a

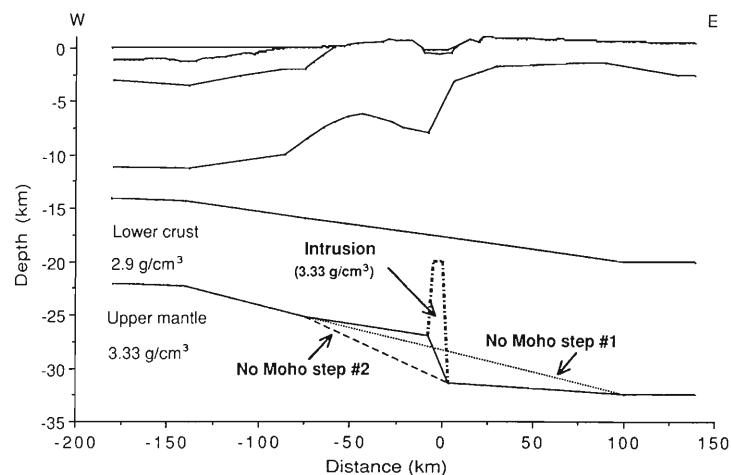


Fig. 6. Alternative density models to investigate the contribution of an intrusion into the lower crust and the requirement for an offset in Moho across the transform. Two possible geometries which eliminate the step in the Moho, marked (1) and (2) were investigated. The modeling results are shown in Fig. 7.

normal crustal thickness of 30–35 km (Ginzburg et al., 1979). The sensitivity of the gravity data to a possibility of a narrow (11 km wide at the base and 5 km wide at the top) (Fig. 6) intrusion of material with an upper mantle density (3.33 g/cm^3) into the lower crust under the rift was also investigated (Fig. 7a). Figure 6 shows that the existence of such an intrusion can be resolved because it introduces a gravity anomaly of up to 15–20 mGal over the median valley and the eastern “rift” shoulder. The bounds for a detectable intrusion can be estimated because the amplitude of the anomaly varies linearly with the change in

density contrast between the crust and the intrusive material and with the average depth of the density anomaly. Thus, an intrusion to a level twice as deep as that shown in Fig. 6 or an intrusion with a density of 3.15 g/cm^3 will probably not be detected.

Discussion

Offset in Moho depth across the transform

The transition in crustal structure across the transform was modeled (Fig. 5) as a fairly abrupt

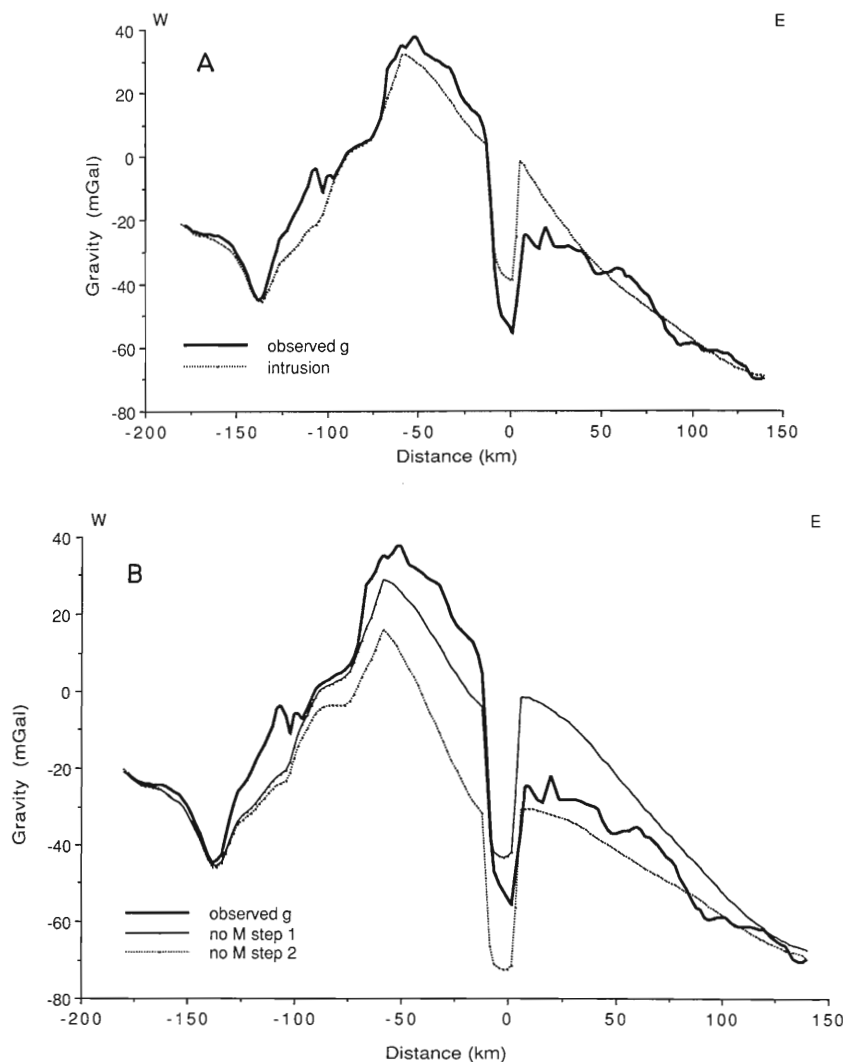


Fig. 7. A. Comparison between the calculated gravity from the model with the intrusion, shown in Fig. 6 (dotted line), and the gravity anomaly (heavy line). B. Comparison between the calculated gravity from the two models in Fig. 6 where the offset in Moho depth is eliminated (dotted and light lines) and the gravity anomaly (heavy line).

step with changes spread over the width of the median valley (about 15–20 km). Although the gravity data cannot constrain the exact geometry of the transition, comparison with two models of a more gradual transition in Moho depth across the transform suggests that a fairly abrupt transition is required. In model (1), the crustal thinning started about 100 km east of the transform (Fig. 6) resulting in a large (up to 25 mGal) mismatch of the Bouguer anomaly and its slope east of the transform (Fig. 7b). In model (2), the crust thickened more rapidly from the Mediterranean toward the Dead Sea transform (Fig. 6) resulting in a large (up to 40 mGal) mismatch of the gravity anomaly west of the transform and under the median valley (Fig. 7b).

The abrupt change in crustal thicknesses across the rift implies that the Dead Sea transform is a relatively narrow zone of deformation which penetrates the entire crust. We suggest that this abrupt change was caused by the 105 km left-lateral movement along the Dead Sea transform. When the profile east of the rift is restored to its original location by 105 km of southward displacement, it is placed against the southernmost part of the Dead Sea. The crustal thickness west of the rift at this place is 28–30 km (Ginzburg and Folkman, 1980), i.e., similar to the 30 km thick crust east of the rift. As expected, then, the crustal thickness across the rift was, probably, continuous prior to the left-lateral motion along the transform.

The existence of an abrupt crust–mantle transition bears on the debate of the Moho as a young feature that may reform or re-equilibrate after a tectonic event. Meissner et al. (1987) pointed out the flat Moho and the remarkable absence of Caledonian and Variscan mountain roots in Europe, and argued that, with the exception of the “transient” Cenozoic orogenic belts, there is a correlation between crustal depth and tectonothermal age. Klemperer (1989) argued for magmatic underplating of the crust in extensional areas such as the Basin and Range of the western U.S. which resulted in an observed flat Moho. Deep seismic profiling of the Late Devonian Redbank thrust zone in central Australia (Goleby et al., 1989) suggested, on the other hand, that Moho topogra-

phy is maintained over a long period of time. There has not been, however, a discussion of crustal reforming after horizontal motion along transform faults which juxtapose different crustal sections across narrow boundary zones. Our gravity modeling of the Dead Sea transform suggests that crustal reforming has not occurred since the Dead Sea transform became active during the Miocene, and an abrupt step in Moho depth is maintained across the transform.

Isostatic compensation of the uplifted rift shoulders

If an ideal state of local isostasy existed, surface topography would be compensated by variable densities and/or layer thicknesses at depth, so that all rock columns above a certain compensation depth are equal in weight (the Airy and Pratt models). The weights of the individual columns along the profile were computed using the densities and the depths to interfaces in the gravity model of Fig. 5 and the eastern end of the profile was chosen as an arbitrary reference column. As shown in Fig. 8, the topography of the “rift-shoulders” is not compensated locally. For example, in order to balance all the rock columns within the profile without changing the shallow and the intermediate structures, the depth to the crust–mantle interface must be considerably greater than that predicted by the gravity model (Fig. 8). Alternatively, densities must be varied laterally within the crust and/or upper mantle. According to an Airy isostatic model the Moho should be at a depth of as much as 33 km west of the rift and 36 km east of the transform. Estimates of Moho depth based on seismic refraction data west of the rift give a depth of 22–27 km (Ginzburg and Folkman, 1980). In order to achieve local isostatic balance east of the transform the elevated eastern shoulder must have a crustal root, in contrast to observations from seismic refraction profiling (El-Isa et al., 1987).

Although the possibility of lateral density variations across the transform cannot be discounted, extensive density heterogeneities of the wavelength suggested by the mismatch of Fig. 7 cannot pass undetected by gravity. Unlike residual gravity anomalies along the San Andreas fault which may

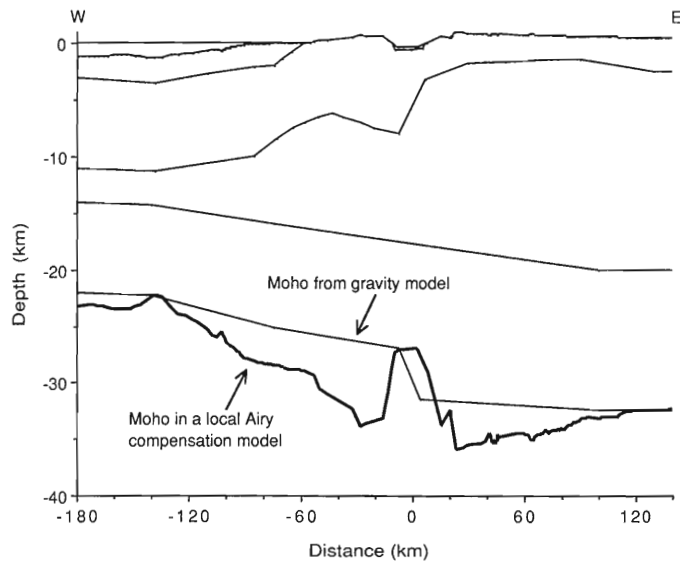


Fig. 8. Comparison between the Moho depth in a local Airy compensation model (heavy line) and the depth to Moho determined by the gravity model of Fig. 5. The Moho in a local Airy model was calculated by computing the weights of the individual crustal columns along the profile with the geometry and density structures of Fig. 5 (thin lines). The vertical column at the eastern end of the profile was taken as an arbitrary reference column.

be attributed to upper crustal density variations due to accretion and subduction (R.W. Simpson, pers. commun., 1989), extensive upper crustal density variations are less likely in the area of the Dead Sea gravity profile. The Levant in the area of the profile was last affected by a Mesozoic

passive continental margin with only small amounts of subsequent compressional folding (Bein and Gvirtzmann, 1977).

Using the subsurface density structure derived from the gravity model of Fig. 5 we can predict the topography that will satisfy a local Airy

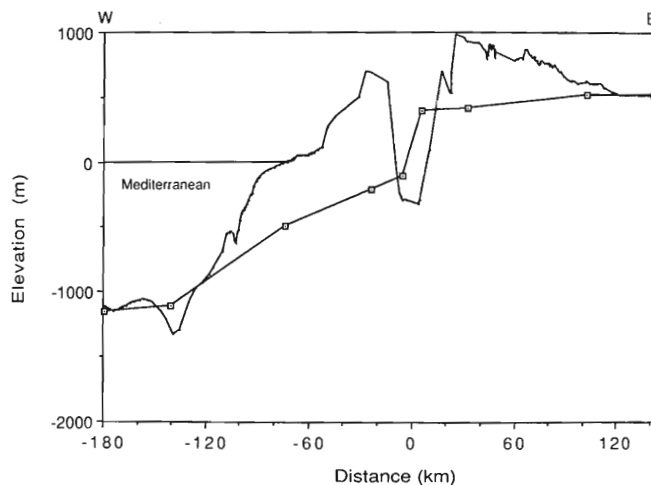


Fig. 9. Comparison between the observed topography along the profile (continuous line) and the predicted elevation in a local Airy compensation model (open squares). The predicted elevation was calculated in a manner similar to that explained in Fig. 8, except that, instead of the Moho, the topography was allowed to vary. The difference between the observed topography and the predicted elevation represents the uncompensated topography and is referred to in the text as the amount of uplift.

isostasy and compare it to the observed topography. Figure 9 shows a large discrepancy between the observed elevation of the rift shoulders and the predicted elevation, assuming local isostasy, in a region of about 100–125 km on either side of the rift. The maximum elevation difference is 500 m east of the rift and 800–900 m west of it. These differences provide an estimate for the amount of shoulder uplift associated with the Dead Sea transform assuming that prior to the development of the transform the profile was locally compensated. The assumption of local isostasy prior to the development of the transform may be inaccurate because passive continental margins may in part possess a finite rigidity (see discussion by Watts, 1988). It is also possible that the short-wavelength (< 30 km) monoclines of the Syrian arc fold were uncompensated. We use the assumption of local isostasy for the sake of simplicity and because the true state of isostasy in the area in the past has not been studied.

The lateral distribution of the deduced uplift is somewhat surprising. It appears that the magnitude of shoulder uplift west of the transform is higher than east of the rift (Fig. 9) in contrast to the higher absolute elevation of the eastern shoulder of the Dead Sea rift compared to the western shoulder. There are three possible explanations for this contradiction: First, the overall “background” elevation of the Arabian plate east of the Dead Sea Rift is 700–900 m above sea level, while west of the transform the “background” elevation can be estimated only for the northern Sinai peninsula, where it is 0–300 m. When these “background” elevations are subtracted from the absolute elevation of the transform shoulders, the western shoulder may indeed be higher. Second, the magnitude of uplift west of the transform may be overestimated because of the existence of Syrian arc topography prior to the formation of the Dead Sea transform (Garfunkel, 1978). Third, the flexural rigidity of the continental margin prior to the development of the transform is expected to have increased seaward (Steckler and Ten Brink, 1986) rendering our basic assumption less valid in the western shoulder than on the eastern shoulder. Apart from an outcrop of marine Pliocene sediments which is now at an elevation of 500 m west

of the Dead Sea basin (Bentor et al., 1965), there are currently no independent estimates for the amount of uplift of the transform shoulders.

Uplift mechanisms

If the present topography of the uplifted shoulders is not compensated locally (and the possibility of undetected lateral density heterogeneities is discarded), the topography should be either compensated regionally or maintained dynamically or a combination of both.

A debate about the causes of the topography of the East African rift shoulders has been continuing for many years. For example, Vening-Meinesz (Heiskanen and Vening-Meinesz, 1958) attributed the rift topography to a mechanical rebound of a rigid lithosphere which was detached along an inclined fault, Banks and Swain (1978) supported the idea of local compensation in the lower crust and upper mantle, and Bechtel et al. (1987) attributed the rift topography to surface and shallow subsurface loading of a rigid lithosphere in the form of volcanoes and dikes. It appears that there are no significant surface loads or thermal sources within the crust in the vicinity of the Dead Sea transform to explain the rift morphology, and the uplift source should either be pushed deeper into the mantle or be mechanical (e.g., the release of accumulated stress or unloading) rather than thermal.

To investigate the possible causes of uplift we tested three simple uplift models of regional isostasy and one model for dynamic support (Fig. 10) and compared their predictions to the deduced uplift. In fitting these models to the uplift we searched for the parameters which minimized the root mean square (rms) difference between the inferred and the predicted uplift. The free model parameters for the models of regional isostasy included the elastic thickness of the plate, the maximum amount of uplift, and the location at which the point force was applied. For the model of dynamic support the half-width of a Gaussian-shaped distributed source was used as a free parameter instead of the elastic thickness, and local compensation was assumed. Comparisons of the four models to the inferred uplift are shown in

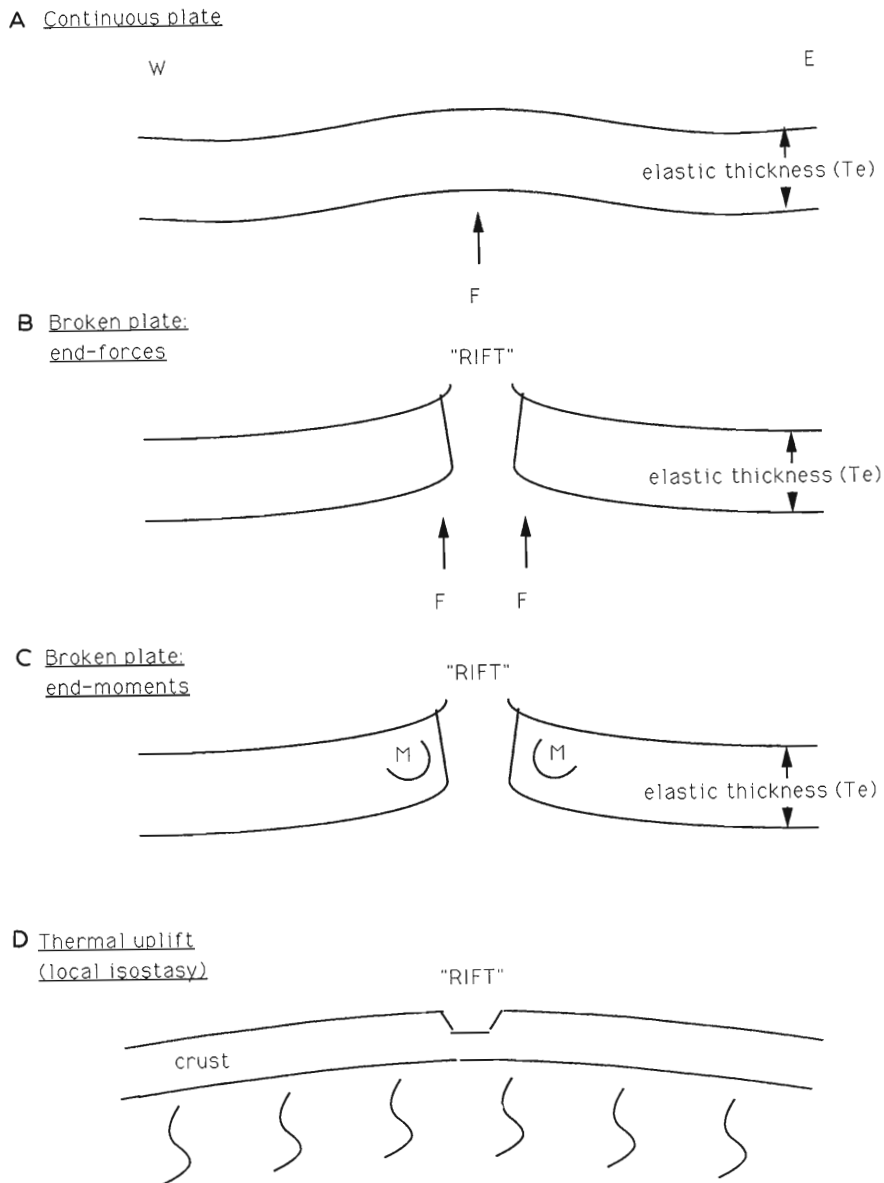


Fig. 10. Cartoon of the four end members of uplift models discussed in the text. The models are: (A) a continuous elastic plate loaded from below, (B) an elastic plate broken along the median valley and the two plate edges loaded separately from below, (C) same as in (B) but the two cantilevered beams are subjected to bending moments within the plates, and (D) a dynamically maintained crust (by a buoyancy force) with a Gaussian distribution along the profile. Isostatic compensation is assumed to be local.

Fig. 11 and the parameters which were used to generate them are listed in Table 1. Rms differences were computed separately for the uplifted shoulders east ($23 \leq x \leq 140$ km) and west ($-180 \leq x \leq -19$ km) of the Dead Sea transform to facilitate the comparison of the match of the different models to the inferred uplift.

The first model assumes that the uplift was caused by a point force which flexed a continuous

elastic plate upward (Fig. 10A). The deflection, $\omega(x)$, is given by:

$$\omega(x) = \omega_0 * e^{-\lambda x} (\cos \lambda x + \sin \lambda x) \quad (\text{Hetenyi, 1946}) \quad (1)$$

where ω_0 is the maximum deflection. The characteristic flexural wave number, λ , depends on the density difference, $\Delta\rho$, between the materials overlying and underlying the plate and on the

TABLE 1

Parameters used to generate the four uplift models

	Western shoulder				Eastern shoulder			
	Te (km)	ω_0 (m)	Location of ω_0^* (km from origin)	rms dif- ference (m)	Te (km)	ω_0 (m)	Location of ω_0^* (km from origin)	rms dif- ference (m)
Continuous	20	900	-15	120	20	900	-15	69
Broken								
(End force)	45	1150	-35	113	25	700	+3	64
(End moment)	105	1050	-10	113	60	700	+3	45
Gaussian	**	750	-25	117	**	750	-25	85

* The median valley is located between -11 km and +8 km from the origin of the profile.

** One sigma width = 50 km.

flexural rigidity, D , via the relationship:

$$\lambda^4 = 4D / [\Delta\rho g]$$

where g is the gravitational acceleration. The flexural rigidity is related to the effective elastic thickness, Te , through:

$$D = E * Te^3 / [12(1 - \nu^2)]$$

where E is Young's modulus and ν is Poisson's ratio.

The point force may represent a narrow buoyancy anomaly due to factors such as excess localized heat, or a rising diapir. The continuous elastic plate model fits the deduced uplift remarkably well (Fig. 11a), except in the median valley. The deviations of the uplift from the model in the western side of the rift may be due to the remnant uncompensated short-wavelength topography of the Syrian arc folds. The parameters for this model (Fig. 11A) include an elastic thickness, Te , of 20–25 km and a maximum uplift of 700–900 m which is located at the western boundary of the median valley. The maximum elevation occurs at the location of the applied point force.

The rms difference between the inferred uplift and the flexural model can be slightly reduced (Table 1) by using a model in which the plate is mechanically decoupled along the Dead Sea transform, i.e., both shear stresses and bending moments are zero (Fig. 10B). In this model an extra free parameter is introduced if we allow different elastic thicknesses across the transform. The use

of broken elastic plate models may be justified if the transform fault penetrates the entire crust (down to 30 km). The solution for a broken plate model with an applied end force is given by:

$$\omega(x) = \omega_0 * e^{-\lambda x} (\cos \lambda x) \quad (\text{Hetenyi, 1946}) \quad (2)$$

The parameters for the broken plate model with applied end force include an elastic thickness, Te , of 25 km east of the transform and 45 km west of the transform (Fig. 11B). The increase in plate rigidity toward the Mediterranean Sea can be explained by the decrease in crustal thickness in a region of laterally uniform geotherms (Steckler and Ten Brink, 1986). An elastic plate thickness of 45 km for the Eastern Mediterranean basin is compatible with its suggested Jurassic age (e.g., Bein and Gvirtzman, 1977). The disadvantage of this model is that the magnitude of maximum uplift and its location (i.e., the location of the applied force) vary significantly between the two sides of the rift (Table 1). The applied point forces at the plate break (Fig. 10B) may represent a thermally generated buoyancy force under the rift, similar to the interpretation of the continuous plate model. Alternatively, it may represent rebound due to lithospheric failure under tension along an inclined fault (Heiskanen and Vening-Meinesz, 1958).

If instead of an upward point force, we apply a bending moment at the end of the plate (Fig. 10C), the rms difference east of the rift is signifi-

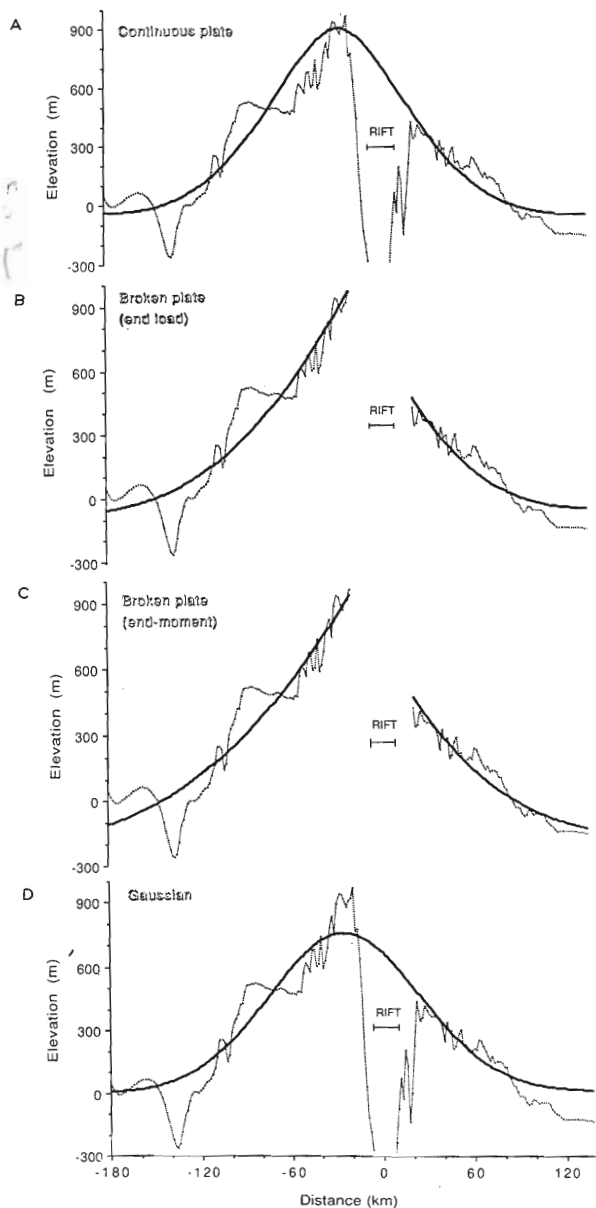


Fig. 11. Comparison between the results from all four uplift models (A–D) of Fig. 10 (continuous line) and the deduced uplift (dotted line). The parameters which were used to generate the models are listed in Table 1.

cantly reduced (Fig. 11C, Table 1). The solution for a broken plate model with an applied end moment is given by:

$$\omega(x) = \omega_0 * e^{-\lambda x} (\cos \lambda x - \sin \lambda x) \quad (\text{Hetenyi, 1946}) \quad (3)$$

Bending moments within an elastic plate are generated when the stress distribution with depth is

not uniform. Thermal bending stresses due to progressive cooling of the oceanic lithosphere away from the mid-oceanic ridge were suggested as a mechanism for generating the characteristic geoid anomaly and part of the topography at fracture zones (Parmentier and Haxby, 1986). The uplift of the Dead Sea Rift shoulders may be attributed to the release of stresses within the Arabian plate as the plate broke along the transform boundary. These stresses could accumulate if the lower lithosphere was heated while the uppermost part of the lithosphere remained relatively cool. Alternatively, these stresses could result from the collision of Arabia with the Iranian subplates. The difficulty with the bending moment model is that the elastic thickness, Te , which is required to fit the inferred uplift, is too large. While an elastic thickness of 60 km east of the rift is within the range of elastic thickness ($Te = 50 \pm 25$ km) determined by Snyder and Barazangi (1986) for the subducted Arabian plate under the Zagros Mountains, a value of $Te = 105$ km west of the rift (Table 1) seems unreasonably high.

We also investigated the possibility that the lithosphere has no rigidity and the shoulder uplift is maintained dynamically by a distributed buoyancy which underlies the entire width of the uplift (Fig. 10D). The buoyancy is generally thought to arise from heat or convective flow perturbations located within or at the bottom of the lithosphere. The shape of this source is unknown, but following other workers (e.g., Detrick and Crough, 1978) we may assume that it has a Gaussian cross section of the form:

$$\omega(x) = \omega_0 * e^{-(x/2\sigma)^2} \quad (4)$$

where σ is the half-width of the source. The maximum uplift in this model (Fig. 11D) (750 m) is located 14 km west of the median valley (Table 1). There is no supporting evidence in the geology (in the form of thermal activity indicators), however, for a westward asymmetry of the heat source.

In summary, the fits of all the above end-member models to the deduced uplift are comparable, and a preferred mechanism for the observed rift-shoulder uplift cannot be distinguished with the current available data. The fit of all models to the shoulder uplift east of the rift is much better than

the fit to the western rift shoulder. The causes of the degraded fit west of the rift are, most probably, the higher expected degree of erosion there (due to the proximity to the base level of the Mediterranean Sea and the higher precipitation rate) and the presence of the cross-cutting structure of the Syrian arc.

Conclusions

The Dead Sea transform ("Rift") displays a unique mixture between continental rift and transform features. The analysis of a gravity and topography profile across the Dead Sea transform suggests the following:

(1) There is no requirement for a significant density anomaly underlying the median valley.

(2) The gravity field along the profile can be explained by two different crustal blocks which have been juxtaposed by the 105 km offset along the Dead Sea transform. The 4–5 km offset in Moho depth implies that the Moho has not re-equilibrated since the formation of the transform, unlike in some examples from both extensional and compressional regions around the world.

(3) The current elevation of the transform shoulders does not appear to be compensated locally. Assuming a state of local isostasy prior to the development of the transform, the magnitude of shoulder uplift (i.e., the uncompensated topography) in the vicinity of 32°N is estimated at 700–900 m and its half-width is 100–125 km.

(4) If the topography is not compensated locally, it should be either compensated regionally or be maintained dynamically. The possible driving forces may include a mechanical force in the form of stress release or an isostatic rebound or an upper mantle thermal source. Predictions from quantitative end-member models do not allow us to distinguish among the suggested mechanisms for shoulder uplift due to lack of better constraints on the uplift.

Acknowledgements

This work was supported in part by a grant from the Israeli Academy of Science. The authors would like to thank Tom Brocher, Bob Simpson

and Gadi Shamir for their thoughtful and extensive reviews, and R. Asael and E. Ram for their help in obtaining the data.

References

- Abu-Ajamieh, M., 1973. Regional gravity map of Jordan. Scale 1:250,000. Natl. Resour. Auth., Amman.
- Banks, R.J. and Swain, C.J., 1978. The isostatic compensation of East Africa. *Proc. R. Soc. London*, Ser. A, 364:331–352.
- Bechtel, T.D., Forsyth, D.W. and Swain, C.J., 1987. Mechanisms of isostatic compensation in the vicinity of the East African rift, Kenya. *Geophys. J. R. Astron. Soc.*, 90:445–465.
- Bein, A. and Gvirtzman, G., 1977. A Mesozoic fossil edge of the Arabian plate along the Levant coastline and its bearing on the evolution of the Eastern Mediterranean. In: B. Biju-Duval and L. Montadert (Editors), *Structural History of the Mediterranean Basins*. Technip, Paris, pp. 95–110.
- Ben-Avraham, Z., Hanel, R. and Villinger, H., 1978. Heat flow through the Dead Sea rift. *Mar. Geol.*, 28: 253–269.
- Ben-Avraham, Z., Almagor, G. and Garfunkel, Z., 1979. Sediments and structure of the Gulf of Elat (Aqaba—northern Red Sea). *Sediment. Geol.*, 23:239–267.
- Bender, G., 1968. *Geologie von Jordanien*. Borntraeger, Berlin, 230 pp.
- Bentor, Y.K., Vroman, A. and Zak, I., 1965. Geological map of Israel. Scale 1:250,000. Southern sheet. Gov. Print., Jerusalem.
- Bohannon, R.G., Naeser, C.W., Schmidt, D.L. and Zimmermann, R.A., 1989. The timing of uplift, volcanism, and rifting peripheral to the Red Sea: a case study for passive rifting? *J. Geophys. Res.*, 94:1683–1702.
- Buck, W.R., 1986. Small-scale convection induced by passive rifting: the cause for uplift shoulders. *Earth Planet. Sci. Lett.*, 77:362–372.
- Detrick, R.S. and Crough, S.T., 1978. Island subsidence, hot spots, and lithospheric thinning. *J. Geophys. Res.*, 83:1236–1244.
- DMA, 1982. Operational navigation chart, sheet G-4. Def. Mapp. Agency, St. Lewis, U.S.A., Ed. 12.
- Dubertret, L., 1970. Review of structural geology of the Red Sea and surrounding areas. *Philos. Trans. R. Soc. London*, Ser. A, 269:9–12.
- El-Isa, Z., Mechie, J., Prodehl, C., Makris, J. and Rihm, R., 1987. A crustal structure study of Jordan derived from seismic refraction data. *Tectonophysics*, 138:235–253.
- Feinstein, S., 1987. Constraints on the thermal history of the Dead Sea graben as revealed by coal ranks in deep boreholes. *Tectonophysics*, 141:135–150.
- Folkman, Y., 1976. Magnetic and gravity investigations of the crustal structure in Israel. Ph.D. Thesis, Tel Aviv Univ.
- Folkman, Y., 1980. Magnetic and gravity investigations of the Dead Sea rift and adjacent areas in northern Israel. *J. Geophys.*, 48:34–39.

- Freund, R., Garfunkel, Z., Zak, I., Goldberg, M., Derin, B. and Weissbrod, T., 1970. The shear along the Dead Sea rift. *Philos. Trans. R. Soc. London, Ser. A*, 267:107–130.
- Furlong, K.P., Hugo, W.D. and Zandt, G., 1989. Geometry and evolution of the San Andreas fault zone in northern California. *J. Geophys. Res.*, 94: 3100–3110.
- Galanis, S.P., Sass, J.H., Munroe, R.J. and Abu-Ajamieh, M., 1986. Heat flow at Zarqa Ma'in and Zara and a geothermal reconnaissance of Jordan. *U.S. Geol. Surv. Open-File Rep.* 86-631, 110 pp.
- Garfunkel, Z., 1978. The Negev Regional synthesis of sedimentary basins. *Int. Congr. Sedimentol.*, 10th (Jerusalem) Guideb. 1, pp. 35–101.
- Garfunkel, Z., 1981. Internal structure of the Dead Sea leaky transform (rift) in relation to plate kinematics. *Tectonophysics*, 80:81–108.
- Ginzburg, A. and Folkman, Y., 1980. The crustal structure between the Dead Sea rift and the Mediterranean Sea. *Earth Planet. Sci. Lett.*, 51:181–188.
- Ginzburg, A. and Folkman, Y., 1981. Geophysical investigation of crystalline basement between Dead Sea rift and Mediterranean Sea. *Am. Assoc. Pet. Geol. Bull.*, 65:490–500.
- Ginzburg, A., Makris, J., Fuchs, K., Perathoner, B. and Prodehl, C., 1979. Detailed structure of the crust and upper mantle along the Jordan–Dead Sea rift. *J. Geophys. Res.*, 84:5605–5612.
- Goleby, Br., Shaw, R.D., Wright, C., Kennett, B.L.N. and Lambeck, K., 1989. Geophysical evidence for “thick-skinned” crustal deformation in central Australia. *Nature*, 337:325–330.
- Hatcher, R.D., Jr., Zeitz, I., Regan, R.D. and Abu-Ajamieh, M., 1981. Sinistral strike-slip motion on the Dead Sea rift: confirmation from new magnetic data. *Geology*, 9:458–462.
- Heiskanen, W.A. and Vening-Meinesz, F.A., 1958. *The Earth and its Gravity Field*, McGraw–Hill, New York, 470 pp.
- Hetenyi, M., 1946. *Beams on Elastic Foundation*. Univ. Michigan Press, Ann Arbor, 255 pp.
- Kashai, E.L. and Crocker, P.F., 1987. Structural geometry and evolution of the Dead Sea–Jordan rift system as deduced from new subsurface data. *Tectonophysics*, 141:33–60.
- Klemperer, S.L., 1989. Deep seismic reflection profiling and the growth of the continental crust. *Tectonophysics*, 161:223–244.
- Kovach, R.L. and Ben-Avraham, Z., 1985. Gravity anomalies across the Dead Sea rift and comparison with other rift zones. *Tectonophysics*, 111:155–162.
- Lachenbruch, A.H. and Sass, J.H., 1980. Heat flow and energetics of the San Andreas fault zone. *J. Geophys. Res.*, 85:6185–6222.
- Makris, J., Ben-Avraham, Z., Behle, A., Ginzburg, A., Giese, P., Steinmetz, L., Whitmarsh, R.B. and Eleftheriou, S., 1983. Seismic refraction profiles between Cyprus and Israel and their interpretation. *Geophys. J. R. Astron. Soc.*, 75:575–591.
- Meissner, R., Wever, Th. and Fluh, E.R., 1987. The Moho in Europe—implications for crustal development. *Ann. Geophys.*, 5B:357–364.
- MOD, 1982. Operational navigation chart, sheet H-5. *Dir. Mil. Surv., Ministr. Def.*, London, Ed. 7-GSGS.
- Moretti, I. and Chenet, P.Y., 1987. The evolution of the Gulf of Suez rift: a combination of stretching and secondary convection. *Tectonophysics*, 133:229–234.
- Parmentier, E.M. and Haxby, W.F., 1986. Thermal stresses in the oceanic lithosphere: evidence from geoid anomalies at fracture zones. *J. Geophys. Res.*, 91:7193–7204.
- Quennell, A.M., 1959. Tectonics of the Dead Sea rift. *Int. Geol. Congr.*, 20th Sess. (Mexico City, 1956), pp. 385–405.
- Scott, D.L., Rosendahl, B.R. and Burgess, C.F., 1989. Comments on “variable extension in Lake Tanganyika” by C.K. Morley. *Tectonics*, 8:647–650.
- Snyder, D.B. and Barazangi, M., 1986. Deep crustal structure and flexure of the Arabian plate beneath the Zagros collisional mountain belt as inferred from gravity observations. *Tectonics*, 5:361–373.
- Steckler, M.S., 1985. Uplift and extension at the Gulf of Suez. *Nature*, 317:135–139.
- Steckler, M.S. and Ten Brink, U.S., 1986. Lithospheric strength variations as a control on new plate boundaries: examples from the northern Red Sea region. *Earth Planet. Sci. Lett.*, 79:120–132.
- Watts, A.B., 1988. Gravity anomalies, crustal structure and flexure of the lithosphere at the Baltimore canyon trough. *Earth Planet. Sci. Lett.*, 89:221–238.